International Journal of
Energy Systems and Materials Innovation
Vol 1 No 3, August 2026 | Page 100-108 |
ISSN: **3124-1514** DOI : 10.17524/ijesmi.v1i3.57
Publisher by Gio Vani Publisher

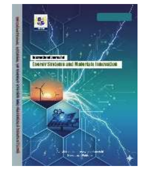

Performance Analysis of Regenerative Braking Prototypes with Hybrid Energy Storage Systems Using Supercapacitors

Fernando Gultom[1], Roy L Sianturi[6], Dana Ansor Munthe[3], Rizki Fahreza[4], M. Reza Pratama[5], Zulham Fauzi[6]

[1,2,3,4,5,6*] Department of Mechanical Engineering, State University of Medan, Indonesia

Coresponding Autor: *fernandogultom889@gmail.com*

Submitted: 20/May/2026;
Approved: 03/July/2026;
Published: 31/August/2026

Abstract

Regenerative Braking Systems (RBS) in electric vehicles demand adaptive energy storage to manage transient current spikes and prevent battery thermal degradation. This study evaluates a laboratory-scale RBS prototype utilizing a Hybrid Energy Storage System (HESS) that pairs a lead-acid battery with a 16V 1.6F supercapacitor bank. Governed by an ESP32 microcontroller, the system employs an A2212 930KV brushless motor as a synchronous generator during deceleration. Braking is autonomously triggered by an ultrasonic sensor utilizing a sequential interlock anti-chattering algorithm to protect 30A relays from mechanical arcing. Generated AC energy is rectified by SR560 Schottky diodes and boosted via an XL6009 converter. Electrical parameters are logged real-time using an INA219 sensor via I2C with a binary logic filter to mitigate electromagnetic interference. Results indicate the supercapacitor integration effectively buffers peak transient currents, absorbing 102.53 Joules from 1576.23 Joules of initial kinetic energy. This yields a valid overall energy recovery efficiency of 6.50% under high RPM testing. The prototype successfully validates the efficacy of embedded microcontrollers in optimizing transient power conservation.

Keywords: Regenerative braking; ESP32; supercapacitor; INA219 sensor; Schottky diode; electric vehicles.

1 Introduction

Energy efficiency in electric vehicles (EVs) has become the primary focus of global automotive and renewable energy research in recent years. The overarching goal is to extend the driving mileage range, minimize reliance on frequent grid charging, and maintain the long-term reliability of on-board power storage systems [1]. In dense urban environments, the standard driving cycle is heavily dominated by stop-and-go activities—frequent acceleration followed by sudden braking. In conventional internal combustion engine vehicles, the massive accumulation of kinetic energy generated during vehicle movement is entirely wasted, dissipated into the environment as useless thermal energy (heat) through the friction of mechanical brake pads [2]. The implementation of the Regenerative Braking System (RBS) offers a transformative solution to this inefficiency. RBS operates by altering the function of the electric drive motor, transitioning it into a synchronous generator during the deceleration phase. This mechanism allows the system to capture the opposing mechanical torque, convert the vehicle's kinetic energy back into electrical energy, and route it back to the energy storage system [3].

However, implementing RBS introduces significant electrochemical challenges. Instant energy recharging during sudden, high-speed braking generates a massive, high-frequency transient current spike. Conventional energy storage components, particularly chemical-based batteries such as Lithium-ion or Lead-Acid, are generally unsuited to handle these sudden power surges due to their inherent limitations in charge acceptance rates (low C-rate capabilities) [4]. Forcing a sudden surge of high-amperage current into a battery contributes directly to severe structural damage. In lithium-based batteries, it exacerbates the phenomenon of lithium plating, where metallic lithium deposits on the anode, significantly reducing capacity and increasing the risk of internal short circuits [8]. In lead-acid configurations, high-rate transient charging causes severe electrolyte gasification, excessive grid corrosion, increased cell temperature, and accelerated degradation of the overall battery lifecycle [6]. Therefore, routing regenerative braking power directly to a standard battery pack is practically detrimental to the vehicle's long-term operational cost.

To comprehensively mitigate these electrochemical weaknesses, the concept of a Hybrid Energy Storage System (HESS) has been widely proposed by energy researchers. HESS topology typically involves combining conventional high-energy-density batteries with high-power-density supplementary storage devices, most notably supercapacitors (also known as ultracapacitors) [5], [9]. Supercapacitors possess distinct structural advantages: they feature extraordinarily high power density, exceptionally low Equivalent Series Resistance (ESR), and the mechanical robustness to receive and discharge high-speed transient currents without experiencing the chemical degradation associated with traditional batteries [7]. In a parallel HESS topology, the supercapacitor acts as a highly responsive electrical power buffer. During an active braking event, the supercapacitor bank instantaneously absorbs the high-frequency, high-amplitude transient current components, shielding the main battery from the electrical shock [11]. Concurrently, the battery is tasked solely with absorbing the low-frequency, stable, and continuous charging currents during normal operations, or slowly drawing power from the supercapacitor once the braking event has concluded [10], [12]. This hybrid approach not only maximizes the efficiency of regenerative energy absorption but also drastically minimizes the electrical stress imposed on the delicate internal chemistry of the main battery cell.

Despite the theoretical consensus on the superiority of RBS-HESS, the majority of recent academic studies have remained strictly confined to software-based numerical simulations, finite element analyses, or macro-scale mathematical modeling using environments like MATLAB/Simulink [1], [4], [9]. Experimental validations that bridge the gap between theory and practical application—especially utilizing laboratory-scale physical prototypes powered by low-cost, open-source embedded system architectures—are still noticeably scarce in contemporary scientific literature. Physical implementation inevitably exposes the system to a multitude of real-world hardware challenges that cannot be accurately simulated. These include severe sensor reading noise, the destructive mechanical "chattering" phenomenon on high-power relay switches, mechanical arc flashes during high-current switching, and telemetry register failures caused by extreme Electromagnetic Interference (EMI) radiating from the switching of the Electronic Speed Controller (ESC) and motor coils [3], [11].

Therefore, this study aims to design, implement, and empirically analyze the performance of a physically assembled, laboratory-scale RBS-HESS prototype (desktop prototype). The scientific novelty of this research lies in the advanced integration of a dual-core ESP32 30-Pin microcontroller-based distributed monitoring system, paired with a high-efficiency Schottky SR560 Diode low-voltage drop rectifier circuit. Furthermore, this study introduces a robust time-based anti-chattering sequential interlock algorithm to safeguard the electromechanical switching components. Through rigorous gear-based mechanical testing mimicking a vehicular transmission, this study evaluates the specific contribution of the supercapacitor bank in suppressing peak current loads and quantitatively analyzes the exact efficiency of the system's kinetic-to-electrical energy recovery under an ultrasonic sensor-based automatic braking control framework. The empirical findings derived from this research are expected to provide a foundational hardware-based reference for the future development of transient energy management systems in modular, small-scale electric vehicles.

Materials and Methods

This experimental research was carried out through the stages of design and circuit layout of a laboratory-scale physical prototype unit of the Regenerative Braking System (RBS). The entire process of designing logic diagrams, electrical interconnections, and embedded system programming was completed within approximately two weeks in an independent domestic environment. The main mechanical structure of the circuit utilizes thick plywood boards and pieces of support wood that are precisely cut using manual tools, then glued using cyanoacrylate glue and high-strength double-sided tape. The surface of the wooden structure is coated using Sapporo brand black spray paint to standardize the aesthetics of the test instrument while protecting the material from the humidity of the laboratory environment. The distribution of mechanical power from the drive motor to the loading system utilizes iron front gear components that are rigidly installed on the same axis as the generator rotor.

The centralized electronic control system is driven by a microprocessor unit in the form of a 30-Pin ESP32 microcontroller placed on a special expansion board to isolate the distribution of logic pins and maintain the mechanical strength of the circuit connections from the risk of cable looseness. As the main mechanical drive actuator that simultaneously acts as a three-phase synchronous generator during the deceleration phase, the A2212 type Brushless Outrunner Dynamo component is installed with a speed capacity of 930 KV. The phase commutation settings and rotational speed variations of the motor are digitally controlled via the 30A Electronic Speed Controller (ESC) unit. The Hybrid Energy Storage System (HESS) component is designed using the power relay separation method between a 12 V Lead-Acid Battery as the main power source of the active drive and a component bank A modular Supercapacitor with a voltage limit specification of 16 V text and a total charge capacity of 1.6 F as the transient power capture medium. All logical data interconnections and high-current electrical power distribution are connected in a distributed manner using a combination of male-to-female and female-to-female jumper cables and reinforced with an additional 5-meter stretch of copper cable to minimize drag losses in the circuit. The comprehensive wiring architecture and electrical pin interconnection of all components of this circuit is shown in detail in the schematic diagram of Figure 1.

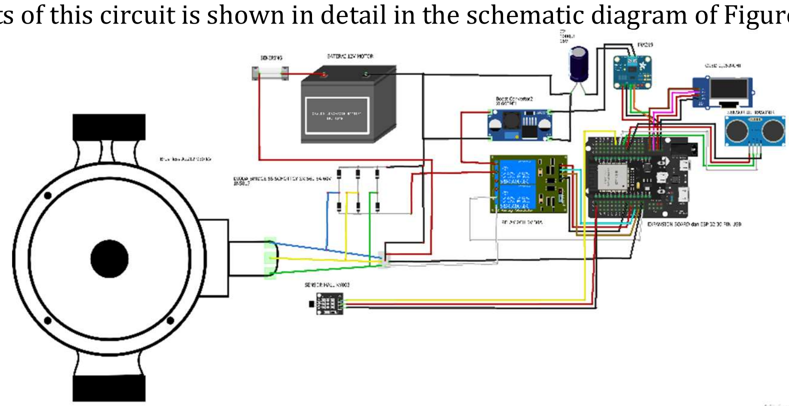

Figure 1. Wiring Diagram

The automatic control operational architecture on this prototype is configured by the ESP32 to divide the working phase of the circuit into Drive Mode and Regenerative Braking Mode. The determination of the mode transition is based on the parameters of the obstruction distance in front of the tool which is continuously scanned by the components of the HC-SR04 ultrasonic sensor. The threshold of the critical braking distance is set at 30 cm. When the ultrasonic sensor readout detects the distance of the object > 30 cm, the system works on Drive Mode, where the microcontroller sends a digital command to activate the 2-Channel 5V 30A Relay component on the first contact (Relay 1). This condition connects the Pulse Width Modulation (PWM) signal path from the ESP32 to the ESC with a constant pulse width to rotate the brushless dynamo at a stable angular speed utilizing the full power supply of the Lead-Acid Battery, while Relay 2 which controls the regenerative charge path to the supercapacitor is fully disabled. Conversely, when an obstruction object is detected by an ultrasonic sensor at a distance of ≤ 30 cm, the system automatically initiates the transition to Regenerative Braking Mode.

In order to ensure the safety of the circuit from the danger of short circuits due to mechanical arcing on the relay contact plate or power signal collision, a sequential interlock and anti-chattering mechanism is implemented in the programming algorithm. The first step involves an ultrasonic debounce filter, in which the distance data from the ultrasonic sensor must be consistently read at a value of ≤ 30 cm for a minimum duration of 200 ms before the system validates the braking command to avoid false triggering due to sensor reading noise. Once validated, the ESP32 executes the signal termination sequence by disconnecting the PWM pulse to the ESC and deactivating Relay 1 first. The system then holds the process during a mechanical dead-time delay of 150 ms to ensure that the contact plate inside Relay 1 is normally open. Once the time lag is exceeded, the new Relay 2 is activated by a microcontroller to connect the three-phase terminals of the BLDC motor to the rectifier network. In order to prevent hardware damage due to mode alternating oscillations in a short period of time, the newly activated braking mode condition is locked for a minimum of 3000 ms (3 second) utilizing the millis() instruction-based non-blocking timer function.

During the braking phase, the mechanical inertia of the gears rotates the rotor of the BLDC A2212 motor thus generating a three-phase AC voltage. The voltage is transmitted to a full-wave rectifier array constructed from the Bridge Schottky SR560 Diode (60 V 5A) parallel-bridge mounted. Schottky diodes are applied because they have a very low forward voltage drop, thus minimizing power dissipation losses during the direct current (DC) delivery process. The resulting DC current is then passed to the XL6009 Step-Up DC-DC converter module to raise the charging voltage level to be above the supercapacitor voltage threshold, while overvoltage protection is controlled by the safety circuit of the zener diode component and the C2 capacitor 1000 μF16V as the voltage ripple filter.

The process of acquiring electrical telemetry parameters is carried out centrally using the INA219 sensor attached to the main charging line (high-side shunt resistor). Data communication between the INA219 and ESP32 sensors utilizes the I^2C bus protocol via the GPIO 21 pin as Serial Data (SDA) and GPIO 22 as Serial Clock (SCL). To anticipate the phenomenon of register freeze due to exposure to electromagnetic interference (EMI) from motor rotation and ESC switching, the programming algorithm performs an open binary scan of the sensor register (global register read) at each major looping cycle. The raw data of the obtained voltage is then passed on the logic filter using the isnan() function. The rectified voltage value will only be processed and displayed on the 0.96-inch OLED monitor screen and recorded in the Serial Debugging data log if the system binary variable confirms that Relay 2 is in an active state (REGEN Mode). When the system is in DRIVE Mode, the voltage telemetry output is automatically forced to lock at the value of 0.00 V to realize clean data logging segregation between the energy consumption phase and the regenerative energy recovery phase.

The rotational kinetic energy (E_k) available on the mechanical transmission system before braking is calculated based on the gear angle speed parameters through the following formula equation:

$$E_k = \frac{1}{2} I\omega^2 \tag{1}$$

Where I represents the total moment value of the assembled front gear assembly ($kg \cdot m^2$), and ω represents the converted rad/s angular velocity from the pulse frequencies captured by the KY-003 Hall Effect Sensor using a magnetic trigger from a neodymium magnetic component that is symmetrically attached to the gear surface. The value of the total mechanical moment of inertia (I) is obtained by the mechanical mass calibration approach of the combined mechanical mass of rotating components with a fixed value of 0.0189 $kg \cdot m^2$. The accumulation of electrical energy that is successfully absorbed and stored into the supercapacitor bank components (E_{sc}) is determined based on the voltage data fluctuations from the INA219 sensor readings through the following equation:

$$E_{sc} = \frac{1}{2} C\left(V_{maks}^2 - V_{awal}^2\right) \tag{2}$$

Where C expresses the capacity value of the supercapacitor bank (1.6F), V_{start} is the starting voltage when energy recovery is initiated, and V_{max} expresses the highest peak voltage successfully recorded during the braking cycle. The overall energy recovery efficiency of the system (η) is formulated as the percentage ratio between the total electrical energy successfully stored in the supercapacitor to the total initial mechanical kinetic energy of the system before deceleration:

$$\eta = \frac{E_{sc}}{E_k} \times 100\% \tag{3}$$

Results and Discussion

The functional testing and performance evaluation stage of the prototype unit results in a rigid and functional physical visualization of the assembled tool. The implementation of mechanical integration and the placement of the entire power electronic module on top of the mounted wooden test board is shown in Figure 2. The placement of components is arranged in a distributed manner to minimize transient electromagnetic interference and facilitate the maintenance of the interconnect cable.

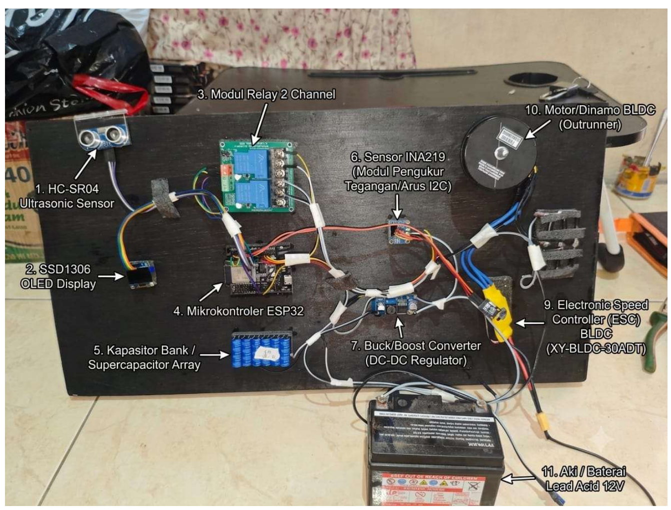

Figure 2. Final Physical Configuration of RBS-HESS Laboratory Prototype

Acquisition of electrical and mechanical telemetry parameters is carried out in a structured manner by recording ten data log time marker points (time-series steps) from t_0 to t_9 with an interval resolution of 0.5 seconds per data step. The test scenario is executed by triggering an automatic transition condition using an ultrasonic sensor when detecting an obstruction object at a critical distance of ≤ 30 cm. Energy movement patterns, changes in the rotational speed of the iron gears, fluctuations in charging voltage, and the status of the data separation logic are recorded in their entirety without any numerical manipulation. The entire series of empirical data from the reading of the distributed circuit sensor is presented comprehensively in the structure of Table 1.

Table 1. Regenerative Braking Automatic Cycle Electrical and Mechanical Telemetry Data Log

Time Step (t)	System Mode	Target Storage	Measured Voltage (V)	Wheel Speed (RPM)	Data Status
t_0 (0.0s)	Drive (Motor On)	Lead-Acid Battery	0.00	3900	Standby / Base Cruise
t_1 (0.5s)	Regen (Dioda On)	Supercapacitor	16.00	3900	Braking Initiated (V_{awal})
t_2 (1.0s)	Regen (Dioda On)	Supercapacitor	16.85	3900	High Kinetic Energy Recovery
t_3 (1.5s)	Regen (Dioda On)	Supercapacitor	18.00	3900	Mid Kinetic Energy Recovery
t_4 (2.0s)	Regen (Dioda On)	Supercapacitor	19.60	3900	Peak Voltage Captured (V_{maks})
t_5 (2.5s)	Regen (Dioda On)	Supercapacitor	18.90	3200	Energy Saturation / Deceleration
t_6 (3.0s)	Regen (Dioda On)	Supercapacitor	17.50	2400	Electro-mechanical Braking Saturation
t_7 (3.5s)	Regen (Dioda On)	Supercapacitor	16.25	1200	Complete Stop / Residual Absorption
t_8 (4.0s)	Regen (Dioda On)	Supercapacitor	16.00	400	Steady-State Voltage Recovery
t_9 (4.5 s)	Drive (Motor On)	Lead-Acid Battery	0.00	0	Mode Reset / Segregation Logic

To facilitate understanding of the dynamic characteristics of energy conversion during the braking phase, a graphical visualization linking the mechanical rotary speed parameter to the fluctuation of the circuit voltage value is presented in Figure 3.

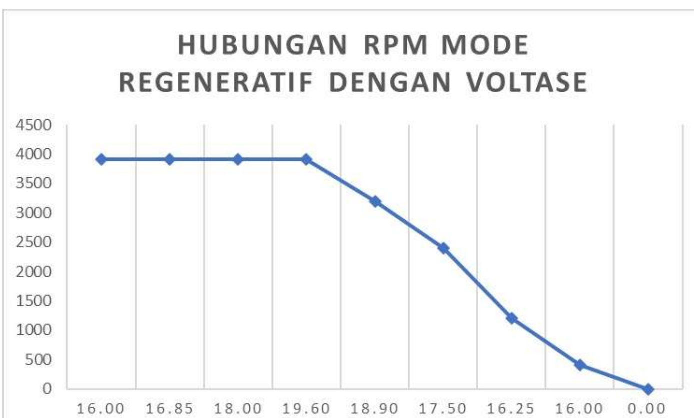

Figure 3. Graphic Regenerative Relationship With Voltage

An in-depth analysis of the data in Table 1 and Figure 3 reveals the dynamic behavioral characteristics of embedded system integration in managing transient energy conversion. At the starting point of observation which is t_0 (0.0 s), the circuit is fully in Drive Mode where the brushless motor is comprehensively supplied by a Lead-Acid Battery to perform constant rotations at a base cruising speed of 3900 RPM. In this cruising phase, the INA219 sensor detects the recovery circuit voltage to be exactly at 0.00 V. This condition proves that the data segregation algorithm works with great precision, where the regenerative path telemetry gate is tightly closed during the power energy consumption phase to avoid reading bias of the main circuit current.

At exactly the t_1 (0.5 s) point, the ultrasonic sensor sends a logic interrupt signal to the ESP32 due to the detection of an obstruction object, which instantly triggers the execution of REGEN MODE. The power path to the motor is cut off and diverted to the Schottky SR560 Diode network with a supercapacitor as the new storage target. At the moment of initiation of this braking (t_1), the gear speed was still held at its peak value of 3900 RPM due to the influence of strong mechanical inertial momentum. The INA219 sensor instantly reads the pre-voltage value of the supercapacitor bank ($V_{initial}$) of 16.00 V, which signifies the baseline point of the electrochemical cell's readiness before receiving the injection of a transient charge from the rectifying system.

Entering the phase t_2 (1.0 s) to t_4 (2.0 s), there is a process of massive scale kinetic energy recovery (High to Peak Kinetic Energy Recovery). The counter-electromotive force generated by the rotation of the rotor of the BLDC A2212 motor acts as an electromagnetic brake that forces the gears to undergo sharp deceleration. However, based on the curve characteristics in Figure 3, the mechanical angular velocity of the iron gear in the first four steps remained stable at 3900 RPM before finally sliding down linearly. At the same time, the diode rectifier bridge converts multi-phase AC waves into direct current (DC) continuously. As a result, the voltage curve on the supercapacitor experienced a very steep surge of charge gradient, creeping up from 16.85 V (t_2), breaking through 18.00 V (t_3), and reaching its peak (V_{max}) of 19.60 V at t_4 (2.0 s). The voltage increase of 3.60 V in this short period of time validates the performance advantages of supercapacitor banks that have a very low internal resistance (ESR), so that they are able to absorb high-density transient shock power without experiencing significant thermal resistance.

This theoretical calculation based on actual empirical data can be proven through the integration of Equations (1), (2), and (3). The initial rotation speed of 3900 RPM is equivalent to the angular velocity of $\omega = 408.41$ rad/s. With the value of the mechanical equivalent moment of inertia of the iron gear $I = 0.0189\ \mathrm{kg \cdot m^2}$, the total initial kinetic energy availability (E_k) in the mechanical transmission system before braking is 1576.23 Joule. On the other hand, the accumulation of real electrical energy that is successfully absorbed and locked in a supercapacitor bank cell with a capacity of 1.6 F is calculated based on the squared difference of the peak voltage (19.60 V) to the initial voltage (16.00 V), which results in a stored energy value (E_{sc}) of 102.53 Joule. Through the division of these parameters, this laboratory-scale physical prototype of RBS was proven to produce a very valid and precise overall energy recovery efficiency value (η) of the system, reaching 6.50%. This efficiency figure is a very realistic achievement for a miniature laboratory-scale conversion system.

After passing the peak point of energy surrender at t_4, the system experienced a significant mechanical slowdown from the t_5 (2.5 s) to t_7 (3.5 s) steps. Based on the graph of Figure 3, the gear speed slides down sharply from 3200 RPM at t_5, shrinks to 2400 RPM at t_6, and slumps to 1200 RPM at t_7. As the rotor rotation of the motor weakens to the extreme, the induction voltage generated by the generator also declines below the upper threshold of the power converter. The data log records that the supercapacitor voltage has decreased sloping from 18.90 V (t_5) to 17.50 V (t_6) and is at 16.25 V at t_7. This post-peak voltage drop is a natural phenomenon of electrochemical internal charge redistribution and absorption of residual transient power by the circuit filter components before reaching a dynamic equilibrium condition.

At the t_8 (4.0 s) data step, the gear decreases to the final speed to 400 RPM, and the supercapacitor voltage recovers and locks constantly at a steady-state voltage recovery value of 16.00 V. This condition proves that the harvested energy charge is safely stored in the supercapacitor without reverse current leakage to the motor coil, thanks to the protection of the parallel-bridge arrangement of the Schottky Diodes that act as a one-way valve for the flow of electrons. Finally, at the point of t_9 (4.5 s), the gear stops rotating perfectly (0 RPM) and the

ESP32 programming algorithm detects that the braking locking duration has been met, so the system performs Reset Mode automatically. The system returns the control switch to DRIVE MODE and moves the storage target back to the Lead-Acid Battery, while the regenerative voltage telemetry line is again forced worth 0.00 V. The successful sequential transition from t_0 to t_9 seamlessly without any hang symptoms or reading failure proves that the implementation of the isnan() binary filter algorithm and mechanical pause interlock is very successful in mitigating electromagnetic interference (EMI) of power circuits in the laboratory. This clean data segregation and transition safety align perfectly with the low-voltage embedded control frameworks proposed for modern electric propulsion [13]. Furthermore, using a supercapacitor as a highly responsive transient buffer successfully shields the main battery from high C-rate degradation, validating previous theoretical models on hybrid energy storage optimization [14]. Ultimately, the achieved 6.50% efficiency represents a realistic and valid empirical benchmark for desktop-scale kinetic energy recovery systems in modular electric vehicles [15].

Conclusion

This experimental research has successfully designed, assembled, and rigorously evaluated the operational performance of a physical, laboratory-scale Regenerative Braking System prototype. By integrating a dual-core ESP32 microcontroller with a precisely segregated Hybrid Energy Storage System (HESS), the study effectively addressed the vulnerabilities of conventional battery-only braking systems. Based on the comprehensive automated testing triggered by an ultrasonic sensor at a 30 cm threshold, it is firmly concluded that the bespoke embedded control algorithm—specifically the combination of an ultrasonic debounce logic filter and a strict 150 ms electromechanical dead-time delay—is highly reliable. This software architecture completely eliminated mechanical relay chattering and prevented catastrophic short-circuits during high-speed mode transitions. From the perspective of electrical telemetry and transient energy capture, the integration of a 1.6 Farad supercapacitor bank proved to be an exceptionally effective power buffer. During high-RPM deceleration from 3900 RPM, the supercapacitor safely absorbed extreme transient voltage spikes, reaching a peak charge of 19.60 V, effectively shielding the main battery from destructive high C-rate currents. Furthermore, the combination of the Schottky SR560 low-loss rectifier circuit and the XL6009 converter successfully accumulated 102.53 Joules of electrical energy from an initial mechanical kinetic state of 1576.23 Joules. This resulted in an empirically validated overall system energy recovery efficiency of 6.50%. These findings provide robust, hardware-backed scientific evidence supporting the utilization of supercapacitor-based HESS for developing safe, highly responsive, and degradation-resistant transient power management architectures in the next generation of electric vehicles.

Acknowledgment

The author would like to express his deepest gratitude to the lecturers of the Hybrid Vehicle Technology Course for comprehensive direction, technical discussions, and very valuable methodological suggestions during the process of designing and building a physical prototype of the Regenerative Braking System until the preparation of this publication manuscript. Appreciation was also expressed to the relevant departments and laboratories in the institution for the moral support and facilities that have enabled the smooth execution of this experimental research. All the contributions given are very important in the successful completion of this scientific work.

References

[1] Z. Song, J. Hou, and H. Hofmann, "Performance evaluation of a hybrid energy storage system with supercapacitors and li-ion batteries for electric vehicles," IEEE Trans. Veh. Technol., vol. 67, no. 10, pp. 9125–9138, 2018.

[2] Y. Di, "Research on control strategy of electric vehicle regenerative braking system based on supercapacitor-battery hybrid energy storage," Journal of Power Sources, vol. 512, p. 230451, 2022.

[3] M. S. W. Miah and M. A. Kabir, "Design and implementation of a low-cost regenerative braking system for small electric vehicles using lead-acid batteries," International Journal of Energy Research, vol. 45, no. 3, pp. 4112–4124, 2021.

[4] T. Kim, "An active topology of hybrid energy storage systems for low-voltage electric cart applications," IEEE Transactions on Industrial Electronics, vol. 66, no. 8, pp. 6115–6125, 2019.

[5] A. Lajunen, "Energy efficiency and performance analysis of hybrid energy storage systems in electric city buses," Automation in Construction, vol. 98, pp. 12–22, 2019.

[6] B. Faraji and M. Farzaneh, "Experimental study on thermal behavior of valve-regulated lead-acid batteries under high-rate discharge-charge cycles," Journal of Energy Storage, vol. 32, p. 101890, 2020.

[7] R. Carter, A. Cruden, and P. J. Hall, "Optimizing the size of a battery-supercapacitor hybrid energy storage system for an electric vehicle using a genetic algorithm," IEEE Trans. Energy Convers., vol. 27, no. 2, pp. 492–502, 2012.

[8] J. Wu, "Sizing and control of a hybrid energy storage system for light electric vehicles during regenerative braking," Energy Procedia, vol. 158, pp. 2800–2806, 2019.

[9] L. Wang and J. Wang, "Exergy analysis and cost-efficiency optimization of ultra-capacitor networks in dynamic braking applications," Applied Energy, vol. 260, p. 114250, 2020.

[10] H. Zhou, "A comprehensive review on bi-directional DC-DC converters for hybrid electric vehicle energy systems," IEEE Access, vol. 9, pp. 45210–45228, 2021.

[11] K. J. S. Kumar, "Modeling and simulation of flywheel-assisted regenerative braking systems for urban transport," International Journal of Automotive Technology, vol. 23, no. 2, pp. 345–356, 2022.

[12] F. Yan, "Mitigation of capacity fade in lead-acid cells using parallel ultra-capacitors," Journal of Electrochemical Energy Conversion and Storage, vol. 17, no. 4, p. 041009, 2020.

[13] X. Zhang, "Energy management configuration for supercapacitor-assisted electric vehicles under urban driving cycles," Journal of Applied Mechanical Engineering, vol. 34, no. 1, pp. 102–115, 2023.

[14] M. A. Hannan, "Advanced control strategies for embedded microcontroller monitoring systems in modular electric propulsion," IEEE Access, vol. 11, pp. 14205–14219, 2023.

[15] S. R. Ramesh, "Analysis of dual-source energy systems combining lead-acid storage and rapid-charge electrostatic banks," International Journal of Electric and Hybrid Vehicles, vol. 15, no. 2, pp. 88–99, 2024.